On the Preferential Location of Al and Proton Siting in Zeolites: A Computational and Infrared Study

German Sastre, Vicente Fornes, and Avelino Corma*

Instituto de Tecnologia Quimica U.P.V.-C.S.I.C., Universidad Politecnica de Valencia, Avenida Los Naranjos s/n, 46022 Valencia, Spain

Received: August 17, 2001; In Final Form: November 9, 2001

Force field atomistic simulations have been used to investigate the Al preferential location and proton siting in zeolites, and the role of the template is shown to be crucial in order to elucidate the Al and acid site distributions. Therefore, it is not the energy of the final structure what controls the Al distribution, but rather the energetics during the synthesis process (zeolite+SDA) that has to be considered, and in this sense the structure directing agent (SDA) accommodation within the microporous space acts not only as a structure director but also as a director of the Al distribution. Once the Al distribution is known, the positively charged SDA can be removed from the calculation and substituted by protons and the population of the four protons in each Al center can be calculated from the corresponding energies. Also, this methodology allows to compute the OH stretching frequencies and, therefore, a map of acid site frequencies, and relative population is obtained which gives a simulation of the OH stretching IR bands in terms of frequencies and intensities. The methodology has been validated by applying this general approach to the case of the newly synthesized ITQ-7 zeolite and the corresponding calculated IR spectrum shows a reasonable agreement with the experimental spectrum. Two bands centered at 3577 and 3624 cm^{-1} result from the simulation, which compare to the experimental values of 3595 and 3629 cm^{-1}. Preferential proton siting has been also studied and energy differences in each AlO_4 tetrahedra of about 30−40 kJ/mol are found, in qualitative agreement with ^1H NMR results.

1. Introduction

Zeolites are crystalline aluminosilicates with regular microporous systems where strong electric fields inside the cavities are responsible for some of the outstanding properties of these materials such as adsorption, ion exchange, and catalytic properties.[1−3] More specifically, the presence of tetrahedrally coordinated framework Al in the silica frame introduces a negative charge in the structure that can be compensated by a proton, and the resultant Brønsted acid site is able to catalyze a large number of reactions proceeding through a carbocation mechanism.[4−5] Different experimental techniques involving adsorption and desorption of bases, as well as ^1H NMR spectroscopy, have been used to characterize Brønsted acid sites in zeolites.[6] Computational methods applied to the study of zeolites, beginning with quantum chemistry methods in the 70s[7] and with force field based methods in the 80s,[8] have also contributed to the understanding of the zeolite OH bond and hence the Brønsted acidity. The early and small cluster models within the quantum chemistry methodology allowed a first characterization of the Brønsted site,[9] and the simulation of larger cluster models, backed by the availability of more powerful computers, allowed to predict changes in the bridging hydroxyl properties over different Al sites.[10] Nevertheless, the cluster model fails to reproduce accurately TOT angles (T ≡ tetrahedral atom) and changes in bond distances upon chemical substitution as a consequence of the considerable flexibility of zeolites. Fixing the cluster boundaries to keep the medium range zeolite structure helps to reproduce TOT angles but does not allow the cluster expansion (or contraction), which is a consequence of the chemical substitution.[11] Additionally, constrained optimizations have been criticized by some research groups under the argument of artifact models.[12] Conversely, full cluster optimization results in better bond distances but precludes reasonable TOT angles to be obtained, and the medium range microporous structure is not reproduced whatsoever. The limitations of the cluster model are critical when one is interested in comparing the physicochemical properties of the OH bond over different Al sites and microporous structures, and in these cases switching to periodic models becomes mandatory. Two methodologies have been developed for this purpose. Quantum chemistry based methodologies without optimization constraints are the first choice if the number of sites to be modeled is sufficiently small.[13−15] Parallel computers are mostly required to perform such calculations, although constrained optimizations and, in particular, the use of symmetry drastically reduce the computational power demand and large unit cells can be modeled.[16] A second approach based on force field (also called *molecular mechanics*) methodologies is also available with the limitation of the semiempirical nature of the calculation, which relies on the quality of (i) the fit to ab initio or experimental data and (ii) the functional form chosen to describe the energy of the system. Despite such limitations, this technique has proven successful in reproducing space groups, cell parameters, bond geometry (or atomic positions), framework vibrations, and lattice compressibility among others.[17] Obviously the quality of these results is lower than that of periodic quantum chemistry calculations, but the substantial gain in computer time (about 2 orders of magnitude) allows a larger set of studies and the possibility of comparison between series of similar materials. For example, a previous study with this methodology allowed the study of 29 different Brønsted acid sites in a MCM-22 unit cell (1×1×2) of 217 atoms with full optimization.[18]

* To whom correspondence should be addressed.

10.1021/jp013189p CCC: $22.00
Published on Web 12/19/2001

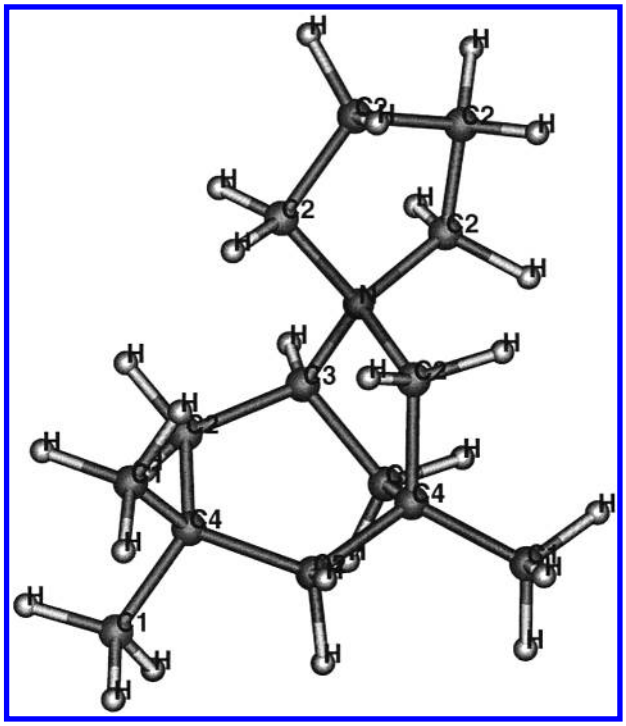

Figure 1. Structure and atom labeling of the organic structure directing agent (SDA) used in the synthesis of ITQ-7, $C_{14}H_{26}NOH$: 1,3,3-trimethyl-6-azonium-tricyclo[3.2.1.4^{6,6}] dodecane hydroxide.

Aluminum distribution in zeolites is a subject of interest as that is characteristic of the Brønsted site location and hence the catalytic properties of the material. Recent studies by Lobo et al.[19−21] have focused on this subject by using different NMR techniques to study the aluminum distribution of Al-ZSM-12 zeolite. They found that the distribution of Al sites is not random but is controlled by the structure directing agent (SDA) used in the synthesis process. The Al sites (a negative defect with respect to a silica framework) tend to locate near the positive charge introduced by the SDA used in the synthesis process. In this way, the SDA has not only the effect of directing the synthesis toward a particular structure(s) but is also responsible for the Al distribution in the as-made zeolite. Recently, the case of ZSM-18 has been studied and the template molecule has been shown to play an important role not only in stabilizing the structure formed but also orientating the Al location in the structure.[22]

In this work we validate the methodology necessary to employ force field computer simulations for the study of Al preferential location and, in particular, the role of the SDA in the Al distributions. To this aim we have chosen the ITQ-7 zeolite. This structure, whose IZA (International Zeolite Association) code is ISV,[23] is a new tridirectional large-pore zeolite, initially synthesized with pure silica composition[24] and more recently with Al incorporated in the structure.[25] It has been shown[26] that under certain conditions ITQ-7 can be synthesized in less than 12 h. The structure is synthesized with the use of two SDAs, an organic cation hosted in the microporous space and an inorganic anion located inside double four ring (D4R) units. We simulate the energetics of the Al distributions and the OH stretching vibrations of the different bridging hydroxyls present in this structure, taking into account the different T positions. The acid strength, stability, and locations of the Brønsted sites in ITQ-7 are simulated within a force field approach, and the calculated OH stretching frequencies are compared to those found experimentally by IR spectra.

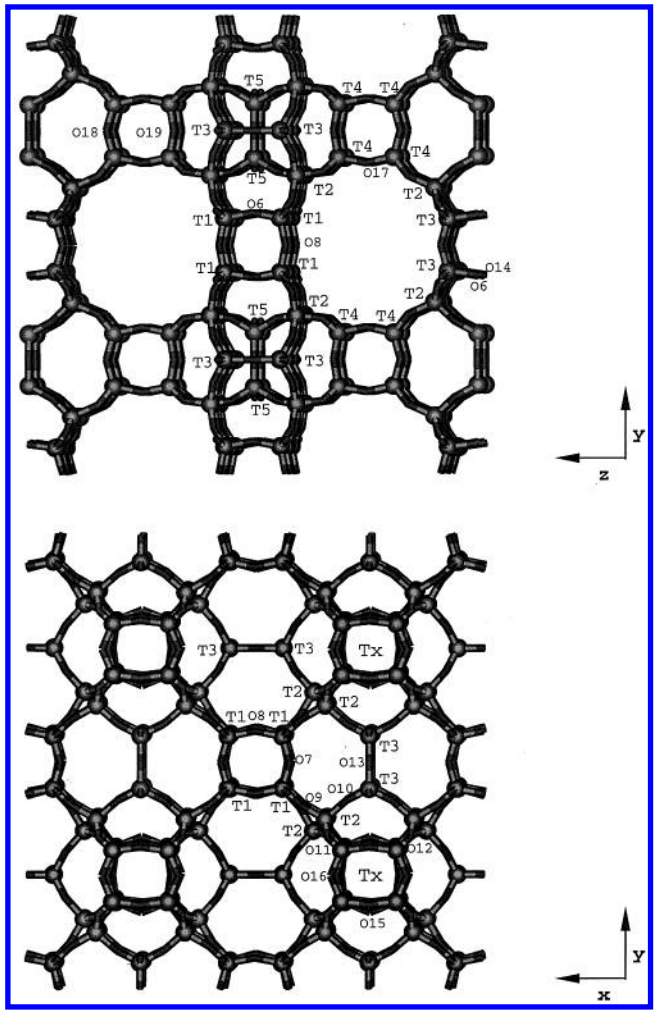

Figure 2. Structure of ITQ-7 showing the five different T sites. T atoms in four rings labeled as "Tx" (bottom figure) can be either four T4 or four T5 types. Three interconnected 12 MR channels are present whose dimensions are: 6.2 × 6.1 Å (parallel to [100] and [010]) and 6.3 × 6.1 Å (parallel to [001]). D4R units are formed either by 8 T1 sites or by 8 T4 sites. The possible acid sites in this structure and their respective location is listed in Table 1.

2. Methodology and Model

The calculations have been performed using lattice energy minimization techniques and the GULP code,[27] employing the Ewald method for summation of the long-range Coulombic interactions and direct summation of the short-range interactions with a cutoff distance of 12 Å. The RFO technique was used as the cell minimization scheme with a convergence criterion of a gradient norm below 0.001 eV/Å. The empirical shell model force field for zeolites[28] has been used throughout. For the calculations including the effect of the SDA in the Al incorporation, the force fields by Kiselev et al.[29] and by Oie et al.[30] have been used for the SDA−zeolite and SDA−SDA interactions, respectively. For the organic SDA, the charge distribution has been obtained by means of the quantum chemistry Hartree−Fock method by using a 6-31G**[31] basis set, and the calculations have been performed by means of the NWCHEM package.[32] Figure 1 shows the different atom types in the SDA and the charges obtained were q(C1) = −0.383 (3 atoms), q(C2) = −0.178 (8 atoms), q(C3) = q(C4) = +0.026 (3 atoms), q(N) = −0.353 (1 atom), q(H) = +0.148 (26 atoms). Electric fields and OH stretching frequencies have been calculated within the GULP code. OH frequencies showed in this work have been corrected by subtracting an anharmonicity constant of 150

TABLE 1: Labeling of the T and O Atoms in the T−O−T Bridges in ITQ-7 as In Ref 20[a]

center	location[b]	center points to: [100]	[010]	[001]
T1−O6−T1	*z*	−	−	1
T1−O7−T1	*xy*	1	1	−
T1−O8−T1	*xyz*	1	1	1
T1−O9−T2	*xyz*	1	1	1
T2−O9−T1	*xyz*	1	1	1
T2−O10−T3	*y*	−	1	−
T2−O11−T5	*yz*	−	1	1
T2−O12−T4	*xyz*	1	1	1
T3−O10−T2	*y*	−	1	−
T3−O10−T2	*y*	−	1	−
T3−O13−T3	*y*	−	1	−
T3−O14−T3	−	−	−	−
T4−O12−T2	*xyz*	1	1	1
T4−O17−T4	*xyz*	1	1	1
T4−O18−T4	−	−	−	−
T4−O19−T4	xyz	1	1	1
T5−O11−T2	yz	−	1	1
T5−O11−T2	yz	−	1	1
T5−O15−T5	−	−	−	−
T5−O16−T5	yz	−	1	1
Total number of centers:		8	16	12

[a] When a Brønsted center is created the corresponding location to which the proton points is also indicated (centers pointing to an unaccessible part are indicated by "−"), and also the total number of centers. [b] *x* − accessible through [100] channels (6.2 × 6.1 Å); *y* − accessible through [010] channels (6.2 × 6.1 Å); *z* − accessible through [001] channels (6.3 × 6.1 Å).

TABLE 2: Coordination Sequence and Multiplicity (in parentheses) of T Sites in ITQ-7 as Labeled in Figure 2 and Ref 20

T1(16)	4	9	18	32	50	71	96	129	167	200	234
T2(16)	4	12	17	30	48	72	99	128	160	199	246
T3(8)	4	11	20	28	42	74	110	132	150	195	258
T4(16)	4	9	18	32	50	72	97	128	167	203	236
T5(8)	4	11	20	28	41	70	105	131	154	188	240

cm^{-1},[33] an average of values obtained from IR measurements of overtone frequencies. More details of the methodology and the force field used can be found in previous studies.[34] The fluor has also been taken into account, and a previously tested force field for fluorine anions in octadecasil, which gives good results, has been used.[35]

ITQ-7 is a zeolite with three interconnected channel systems of 12 MR (membered ring): two of them are of the same size and shape (6.2 × 6.1 Å) and run through the directions [100] and [010]. The third 12 MR system runs parallel to [001] and is formed by windows of 6.3 × 6.1 Å (Figure 2).

The refined tetragonal $P4_2/mmc$ structure of pure silica ITQ-7[24] was used as a starting point and then minimized without symmetry constraints. Then, a single Al atom was introduced in the unit cell to create a Brønsted site, and the resulting cell was again minimized. The Al atom was introduced in each of the five T (tetrahedral) positions of the ITQ-7 structure (Figure 2), and the proton was placed in all the four unequivalent oxygen atoms linked to the corresponding Al. This gives 20 different possibilities having T−O−T labeling as given in Table 1. The connectivity sequence of the ISV structure, which characterizes the different T sites, is shown in Table 2. The labeling corresponds to that used in the original publication of the structure.[24] The centers can point to one or more channels and they are labeled as shown in Table 1, where the number of cases is also indicated. From this counting it can be seen that, in a random distribution over the possible sites there would be more acid centers in the channels parallel to [010] and [001] than in the [100] channels.

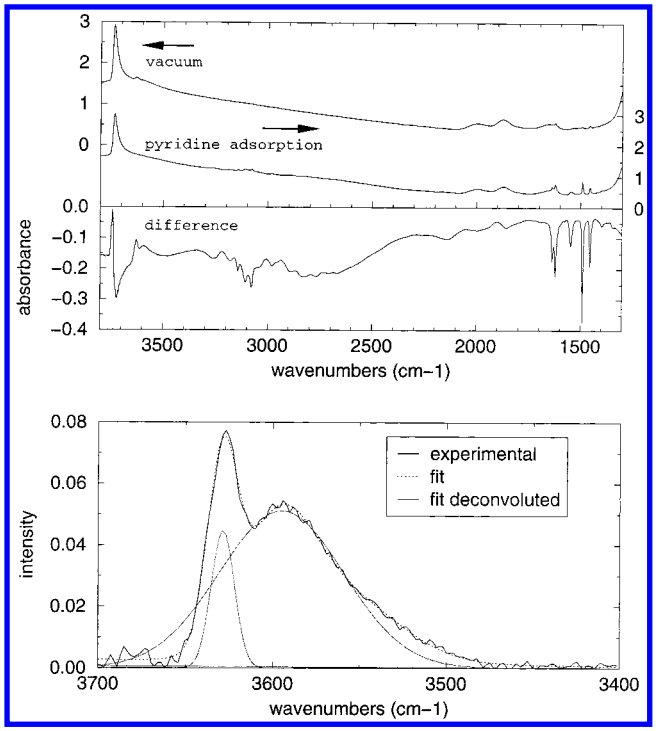

Figure 3. IR spectra of H−ITQ-7 in the OH stretching region. Top: after treatment at 673 K in a vacuum, after adsorption of pyridine, and difference spectrum. Bottom: fit and deconvolution of the hydroxyl spectrum considering Gaussian bands.

3. Experimental Section

A sample of zeolite ITQ-7 with a bulk Si/B ratio of 50 was prepared following the methodology described in ref 25. More specifically, a boron-containing ITQ-7 sample was synthesized first from a gel with the composition $SiO_2/B_2O_3/C_{14}H_{26}NOH/HF/H_2O$ in a molar ratio of 1:0.01:0.5:0.5:3, where $C_{14}H_{26}NOH$ is 1,3,3-trimethyl-6-azonium-tricyclo[3.2.1.$4^{6,6}$] dodecane hydroxide. The gel was prepared by dissolving H_3BO_3 (0.08 g) in a solution of $C_{14}H_{26}NOH$ (0.99 M, 31.98 g). Tetraethyl orthosilicate (TEOS, 13.46 g) was then hydrolyzed in the solution, and the mixture was stirred gently to completely evaporate the ethanol formed. Finally, HF (1.34 g, 48.1% in water) and purely siliceous ITQ-7 crystals (0.20 g) were added and the mixture was homogenized. After a crystallization time of 7 days at 433 K in a PTFE-lined stainless steel autoclave rotating at 60 rpm, a powder was obtained that after washing, drying, and calcining (853 K) yielded a material whose XRD corresponds to that of ITQ-7. In a following step boron was exchanged with Al, and the final material showed by ^{27}Al MAS NMR that Al was tetrahedrally coordinated. The Si/Al ratio as determined by chemical analysis was 50.

For IR spectroscopic measurements of the H−ITQ-7 sample, a 10 mg cm^{-2} self-supported wafer of the sample was introduced in a cell and it was heated at 673 K in a vacuum (10^{-3} Pa) during 14 h. Then the sample was cooled at room temperature and the IR spectrum was registered (Figure 3, top). After this, a pressure of 5×10^{-2} Pa of dry pyridine was admitted in the cell at room temperature and, after adsorption was completed, the sample was heated at 523 K in a vacuum for 1 h to remove the excess of base (Figure 3, top).

TABLE 3: Calculated Equilibrium AlOSi Angle (degrees), Relative Energy (kJ/mol), Population (according to eq 1 within the model in section 4.2.1), and Stretching OH Frequency (cm^{-1}) of the Brønsted Acid Sites Originated from the Substitution Si→Al,H in ITQ-7[a]

types Al−*xx*−Si	angle (Al−O−Si)	relative energy	population	ν_{OH}
T1−O6−T1	147	8.9	0.016	3560
T1−O7−T1	136	3.4	0.147	3627
T1−O8−T1	133	9.3	0.013	3625
T1−O9−T2	139	43.9	0.000	3576
T2−O9−T1	138	41.2	0.000	3565
T2−O10−T3	132	3.0	0.179	3622
T2−O11−T5	130	0.0	0.581	3616
T2−O12−T4	137	31.9	0.000	3567
T3−O10−T2	132	13.7	0.002	3582
T3−O10−T2	132	13.7	0.002	3582
T3−O13−T3	144	28.9	0.000	3543
T3−O14−T3	143	39.9	0.000	3630
T4−O12−T2	138	47.1	0.000	3576
T4−O17−T4	135	16.9	0.001	3606
T4−O18−T4	144	13.0	0.003	3577
T4−O19−T4	134	6.0	0.053	3624
T5−O11−T2	137	14.8	0.001	3560
T5−O11−T2	137	14.8	0.002	3560
T5−O15−T5	148	36.6	0.000	3869
T5−O16−T5	144	21.9	0.000	3551

[a] The AlOSi angles refer to the Brønsted site, AlO(H)Si.

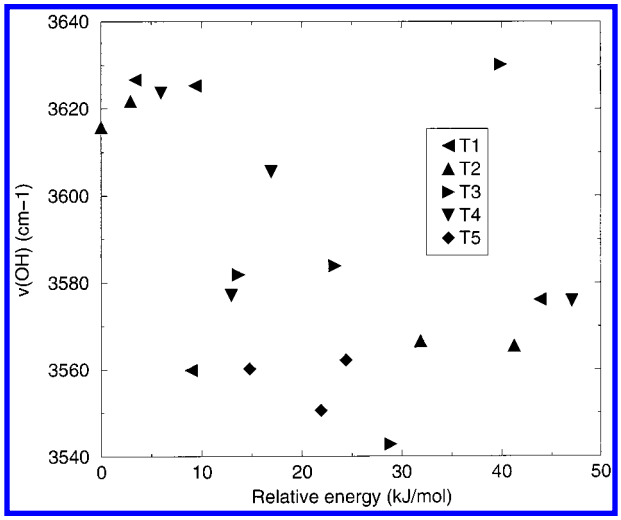

Figure 4. Plot of ν_{OH} stretching frequency (cm^{-1}) versus substitution energy (Si→Al,H) relative to the most stable (kJ/mol). The Al location in each corresponding center is also indicated (T1−T5).

4. Results and Discussion

4.1. Calculated OH Stretching Frequencies. The calculated OH stretching frequencies, ν(OH), for all bridging hydroxyls are shown in Table 3. All the values are within the range 3540−3640 cm^{-1}, except that corresponding to the center Al5−O15−Si5 for which a frequency of 3869 cm^{-1} is obtained. The final acidity of the zeolite is related not only to the resultant OH frequencies but also to the relative occupation of sites in the different crystallographic positions. This distribution depends on the Al substitution energies, which are shown in Table 3. A first estimation of the acidity can be obtained by plotting the OH stretching frequencies against the substitution energy of the corresponding acid site, as shown in Figure 4. The energy span of the substitution energy is nearly 50 kJ/mol, and this is a difference large enough to consider that preferential substitution may take place in this zeolite. It is seen from the results (Figure 4) that two IR bands may be observed in the structure: one near 3620 cm^{-1} (*weaker* centers) and the other at 3570 cm^{-1} (*stronger* centers). The calculated intensities of these bands will determine whether they are observed or not, and this will be given by the corresponding populations that we analyze below.

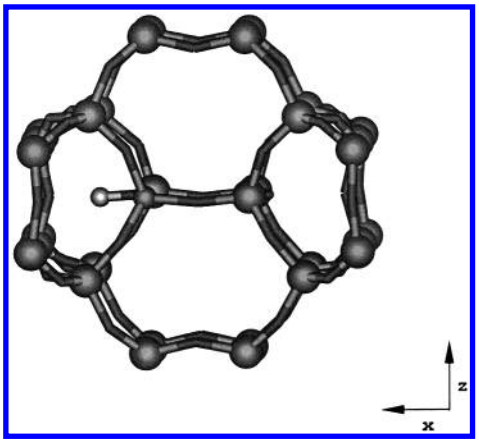

Figure 5. Detail of the Brønsted center siting on the Al5−O15−Si5 site showing its proximity (1.61 Å) to a nonbonded oxygen atom. When the proton is being detached it comes closer to the opposite O atom, which makes the deprotonation energy to decrease substantially, and this makes the acid strength to decrease accordingly. This is the reason for the large OH stretching frequency observed (3869 cm^{-1}, in Table 3).

The high frequency of 3869 cm^{-1} is due to the location of the corresponding proton (Figure 5), neighbor to a nonbonded oxygen atom (1.61 Å) forming part of a ring with 5 oxygen atoms, two of which are located in front of each other, and one of them corresponds to the acid site. In the deprotonation process, as this proton detaches from the corresponding oxygen it also approximates to the opposite oxygen, thus making the total energy to remove the proton considerably larger. This makes the deprotonation energy higher, which results in a lower acidity and therefore a higher OH stretching frequency. This center is located in an unaccessible part of the ITQ-7 structure and is not expected to be involved in catalytic events. Furthermore, its calculated population, as we will see below, is negligible, which explains why a band near 3869 cm^{-1} is not detected experimentally.

4.2. Population of OH Bands. *4.2.1. Model 1: Al Siting Calculated without Taking into Account the Presence of the SDA.* To assess the band population it is necessary to know the relative occupation of the acid centers. With the energies shown in Table 3, the relative occupation of each center can be estimated through the Boltzmann statistic factor:

$$P_i = \frac{e^{-E_i/kT}}{\sum_j e^{-E_j/kT}} \quad (1)$$

Here, the different states are each of the 20 acid centers considered in our study whose energies are listed in Table 3. The site populations are listed in Table 3 and the sum of the 20 populations gives the whole probability. The OH frequency histogram is shown in Figure 6 (bottom), and it can be seen that this model predicts the existence of only one IR band located near 3620 cm^{-1}, as the other frequencies have very low population. In this case we have considered that the probability of the proton to be in a given site is a function of the total energy, and therefore we are not taking into account the interaction of the zeolite atoms with an SDA molecule, i.e., only the final state of the system is considered.

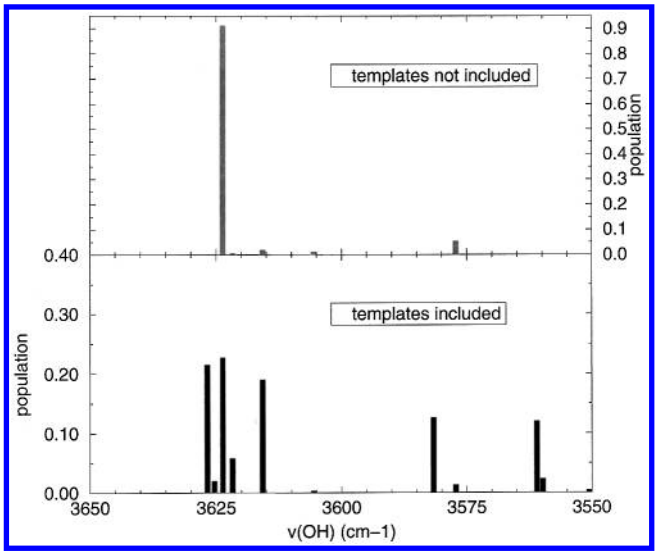

Figure 6. Population of the different OH frequencies found in H−ITQ-7 considering no preferential Al substitution (bottom) and preferential Al substitution (top). The latter model gives a distribution similar to the IR experiments, whereas the former predicts only one hydroxyl band.

4.2.2. Model 2: Al Siting Calculated Taking into Account the Presence of the SDA. It is more accurate to think that protons locate on a specific site after the Al has been introduced in the structure. The synthesis proceeds in a two-step basis: (i) incorporation of the SDA into the void structure plus incorporation of Al (through a Si→Al substitution), compensating the charge of the SDA and (ii) charge compensation by a proton after the charged SDA is calcined. The Al incorporation must then be governed by preferential location according to the energetics of the Al positions (in the presence of the SDA), and therefore different populations for the Al sites are expected. As protons are forced to locate on an oxygen atom in the AlO_4 tetrahedra, this means that the proton populations on a particular oxygen do first depend on the population of the corresponding Al site, and second on the probability distribution of the four oxygens corresponding to the Al site referred. Therefore, the final proton populations will be the product of each probability as follows:

$$P_{ij_i} = P_i P_{ji} \begin{cases} i = 1,2,3,4,5 \text{ (Al positions)} \\ j_i = 1,2,3,4 \text{ (O position for each Al position)} \end{cases}$$

$$= \frac{e^{-E_i/kT}}{\sum_{k=1-5} e^{-E_k/kT}} \cdot \frac{e^{-E_{ji}/kT}}{\sum_{k=1-4} e^{-E_{ki}/kT}} \quad (2)$$

where the subscript i refers to the five Al locations, and the subscript j_i refers to the four oxygens of the corresponding i Al location. Clearly the following relations are obeyed:

$$\sum_{i=1-5} P_i = 1 \quad \text{(Al can be located in five T positions)} \quad (3)$$

$$\sum_{j=1-4} P_{ji} = 1$$

(H in a given Al position can be located on four O) (4)

The whole probability for all the configurations is given by

$$\sum_{i j_i} P_i P_{j_i} = \sum_i P_i [\sum_{j_i} P_{ji}] = \sum_i (P_i \cdot 1) = 1 \quad (5)$$

To calculate the first factor (first term in eq 2), which corresponds to the Al location in the presence of the SDA, a complete study has been performed as detailed below.

The synthesis of ITQ-7, as described in the Experimental Section, was carried in the presence of two structure directing agents: $C_{14}H_{26}N^+$ and F^-. The first occupies the microporous space of the structure, and the fluorine anions locate inside the D4Rs (double four rings) of the structure. Both agents do influence the Al location due to electrostatic effects: the Al acts as a negative charge in a silica network and tends to locate nearby the organic SDA and far away from the negative charge of the fluorine anions. The balance of these two electrostatic factors makes a part in what decides the preferential Al location which is the total energy. The other part of the total energy comes from covalent factors related to the T−O and O−T−O bond and angle strains caused by the incorporation of Al in the different sites of the structure. The complex balance between these two contributions will finally decide the energetics of the process and therefore the Al distribution. To model this in the most accurate way we have started with a unit cell containing one Al atom, so that interaction between centers does not influence the results, and also because the experimental sample contains 1.25 Al per u.c. According to the experimental results,[25] four organic SDAs fit into the microporous void space of the ITQ-7 unit cell, and considering only one Al atom, the electroneutrality requires the presence of three fluorine anions. On the other hand, there are four D4Rs in the unit cell, two of them made by T1 atoms and two by T4 atoms. Two fluorine occupations have been considered: T1-T1-T4, and T1-T4-T4, this meaning that the three fluorine atoms have been located in two D4Rs of the T1 type plus one T4 type (T1-T1-T4); and one fluorine in a T1 type D4R plus two fluorine in D4Rs of the T4 type (T1-T4-T4), respectively. With each one of the two distributions, the Al atom has been placed in each of the 64 possible T locations, which gives 64 Al distributions for each fluorine distribution. Previously, the four organic SDA molecules have been optimized in the ITQ-7 unit cell considering a charge distribution in the SDA atoms giving a neutral total charge and a pure silica ITQ-7 cell. This has been done by taking into account that the SDA fits tightly in the microporous space of the ITQ-7, and therefore the van der Waals interactions can give us a first estimation of the SDA minimum energy positions. In this optimization all the atoms of the zeolite and the SDA have been relaxed. Three SDA orientations into the void space have been tested, and from these the minimum energy orientation has been selected henceforth. The results of these optimizations are given as Supporting Information of this study for the sake of brevity. Once the four organic SDA molecules have been optimized in the microporous space, the Al distributions have been calculated. In each case, an Al atom has been placed in a tetrahedral position and a fluorine anion distribution has been considered. All the atoms of the system have been allowed to relax in order to find the minimum energy of the corresponding distribution. The final results are available as Supporting Information to this study. Regarding the relative energies of the distributions, two conclusions are drawn: (a) the fluorine distribution 2, corresponding to T1-T4-T4, is more stable than the distribution 1, overall. Obviously, there are conformations of the distribution T1-T1-T4 that are lower in energy than many Al locations of the conformation T1-T4-T4, but, overall, the latter fluorine distribution is lower in energy; (b) the total probabilities for each corresponding T site are calculated from those results by summation of the corresponding centers, this giving populations 0.258, 0.247, 0.125, 0.241, and 0.123 for

TABLE 4: Calculated Populations of Al in Each of the Five TO_4 Tetrahedra (P_i), Populations of the Proton Locations in Each T Site (P_{ji}), and Total Populations (P) of the Proton Locations in H−ITQ-7 According to the Model outlined in Section 4.2.2 and eq 2

T site	probability factor (P_i)	AlSi	probability factor (P_{ji})	probability factor ($P=P_iP_{ji}$)	ν_{OH}
T1	0.258	T1−O6−T1	0.090	0.023	3560
		T1−O7−T1	0.834	0.215	3627
		T1−O8−T1	0.076	0.020	3625
		T1−O9−T2	0.000	0.000	3576
T2	0.248	T2−O09−T1	0.000	0.000	3565
		T2-O10−T3	0.235	0.058	3622
		T2−O11−T5	0.765	0.190	3616
		T2−O12−T4	0.000	0.000	3567
T3	0.127	T3−O10−T2	0.499	0.063	3582
		T3−O10−T2	0.499	0.063	3582
		T3−O13−T3	0.001	0.001	3543
		T3−O14−T3	0.000	0.000	3630
T4	0.243	T4−O12−T2	0.000	0.000	3576
		T4−O17−T4	0.011	0.003	3606
		T4−O18−T4	0.055	0.013	3577
		T4−O19−T4	0.934	0.227	3624
T5	0.124	T5−O11−T2	0.482	0.060	3560
		T5−O11−T2	0.482	0.060	3560
		T5−O15−T5	0.000	0.000	3869
		T5−O16−T5	0.035	0.004	3551

T1−T5 overall Al occupations, respectively. These values are listed in Table 4, and are very different from those obtained in Model 1, which means that the SDAs really make an important and unmissable contribution to the Al location. It is seen from these results that the populations of Al atoms located in D4Rs, which correspond to T1 and T4 atoms, are 0.258 and 0.243 (Table 5), which amounts to 0.501. This means that 50% of the Al atoms are expected to be found in the D4R units.

The second probability factor in eq 2 is also calculated, and this refers to the probability distribution of a proton on a given AlO_4 tetrahedra. The energies considered were already calculated (Table 3), but this time the denominator of the Boltzmann expression (denominator of the second factor of eq 2) extends only to four sites (in each AlO_4 tetrahedra). The results (P_{ji}) are given in Table 4. Finally, with both factors calculated, the corresponding product, which is the site population (P), is also calculated and listed in Table 4. A graphic representation of the site populations is given in Figure 6 (top), and it can be seen that, overall, two OH bands appear around 3620 cm^{-1} and 3575 cm^{-1} that will be further analyzed. This model fits better the experimental IR spectrum than the previous model 1 shown in Figure 6 (bottom) where only one band was present. Finally, we find from Table 4 that the most populated Brønsted sites are Al4−O19−Si4, Al1−O7−Si1, Al2−O11−Si5, Al3−O10−Si2, Al5−O11−Si2 and, from the data listed in Table 1, these centers point to the channels in *xyz*, *xy*, *yz*, *y*, *yz*, respectively. From these results it is clear that the *y*-channel, [010], is expected to host a large number of acid sites. It is also noted that the two most populated sites, Al4−O19−Si4 and Al1−O7−Si1, have their T atoms located in D4Rs, although the protons are pointing not to the D4Rs but to the microporous cavities.

4.3. Experimental IR and Simulated OH Stretching Frequencies. The theoretical results obtained can now be compared with the experimental IR spectrum of the H−ITQ-7 in the OH stretching region (Figure 3, top: difference spectrum; and Figure 3, bottom). In this spectrum, three bands at 3745, 3629, and 3595 cm^{-1} can be observed. The first band is assigned to external silanol groups and the other two should be attributed to bridging (acid) hydroxyl groups as they vanish upon pyridine adsorption (see Figure 3, top). The difference spectrum before and after pyridine adsorption (Figure 3, top) shows the IR bands corresponding to acid hydroxyls. Deconvolution of this spectrum (Figure 3, bottom) allows us to say that in the acid form of ITQ-7 there are, at least, two types of bridging hydroxyl groups showing IR bands of very different bandwidth. The bands at 3595 and 3629 cm^{-1} show bandwidths of 75 and 18 cm^{-1}, respectively. This indicates that each IR band should be formed by the superposition of different bands corresponding to slightly different OH groups.

The five more populated calculated frequencies appear at 3560, 3582, 3616, 3624, and 3627 cm^{-1}. The intensities, which are given by the probability factor (P in Table 4), allow us to make a simulation of the bandwidths in order to perform a comparison with the experimental spectrum. For doing that we have performed a fit in which we have considered that the calculated intensities (population) are in relation with the peak area. A constrained optimization was performed trying to keep the frequencies as close as possible to the calculated frequencies, being allowed to move ±6 cm^{-1}. The peak areas were kept fixed to the values given by the populations in Figure 6 (top) and Table 4. The final result (Figure 7) shows a reasonable agreement with the experimental spectrum. In this case, two bands with frequencies at 3577 and 3624 cm^{-1} are obtained and the relative areas are 1.0:2.7, respectively. Differences in relative intensities of the two OH bands can be expected if we take into account the fact that the experimental results have been obtained after calcination of the zeolite to eliminate water and the SDA. Calcination makes a nonnegligible dealumination, and this loss of framework Al could be inequivalent in the different structural Al positions.

4.4. Proton Hopping over AlO_4 Tetrahedra. Once a proton is located next to an Al site, its location can dynamically change over the four O atoms of the tetrahedral Al. The time spent by a proton on each O depends on the configurational energy and the corresponding populations have been calculated (P_{ji}, in Table 4). The energy differences are displayed in Figure 8, and it can be seen that there is a wide span of about 30−40 kJ/mol in the proton energy over the four available oxygen atoms, regardlesss of the Al site type considered (Al1−Al5). In faujasite, where proton location has been measured by neutron diffraction, one proton location has been found to be unoccupied,[36] and this is explained by the high energy difference between the locations, as found in these calculations on ITQ-7. Also, ^1H MAS NMR

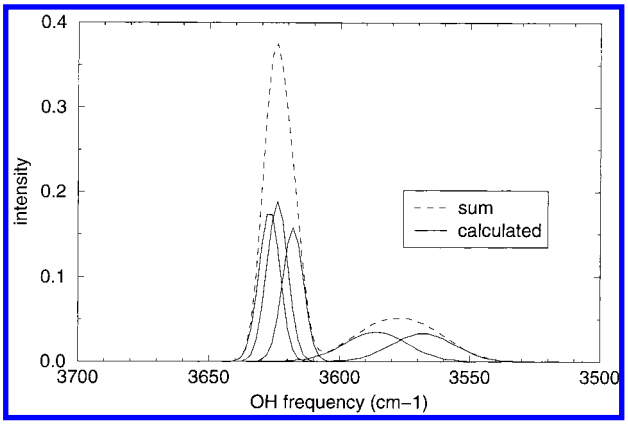

Figure 7. Simulated IR spectrum of the H−ITQ-7 structure with Si/Al = 63 (1 Al/u.c.). The five peaks with largest population have been considered from the data of Table 4, which correspond to the frequencies 3560, 3582, 3616, 3624, and 3627 cm^{-1}, and the relative intensities are obtained from the respective populations. A certain constrained optimization has been performed in order to find the overall shape of the IR spectrum (labeled "sum" in the figure), allowing the frequencies to move ±6 cm^{-1}, whereas the intensities were kept fixed. Two bands with frequencies at 3577 and 3624 cm^{-1} and relative areas 1.0:2.7 are obtained.

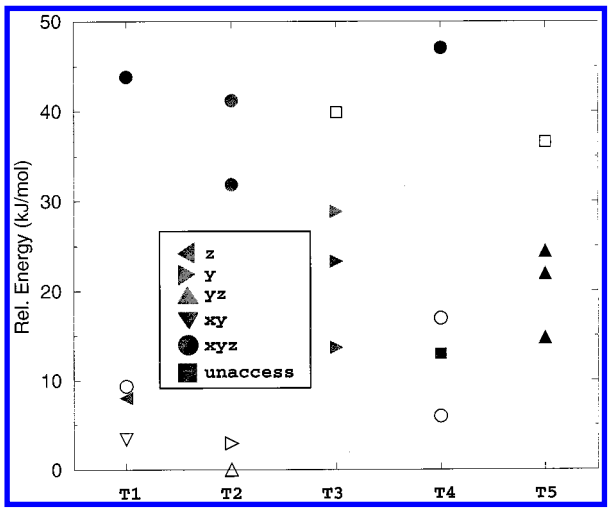

Figure 8. Plot of Si→Al,H substitution energy (kJ/mol) versus Al substitution site. The energies are relative to the minimum (which corresponds to the center Al2−O11−Si5). Four possibilities of placing the proton around each Al atom exist. The environment to which each proton points is also indicated in the graph according to the notation followed in Table 1. Open symbols indicate weaker centers (those above 3600 cm^{-1}) and filled symbols indicate stronger centers (those below 3600 cm^{-1}).

studies have found activation energies for the proton hopping of 45, 54, and 61 kJ/mol in ZSM-5, Mordenite, and Y zeolite respectively,[37] in agreement with the energy differences found here. A recent quantum chemistry study estimates the activation energy for the proton transfer O1→ O4 in faujasite as 86 kJ/mol.[38] These experimental and theoretical results strengthen our conclusion that preferential occupation of protons on a given Al site is expected in ITQ-7.

5. Conclusions

Atomistic simulation techniques have been used to study the Al distribution in zeolite ITQ-7. The experimental infrared frequencies of the H−ITQ-7 bridged hydroxyls associated with the presence of Al have been reproduced by the calculations, and two bands centered at 3577 and 3624 cm^{-1} are found in the simulations, which compare well to the experimental values of 3595 and 3629 cm^{-1}. The energy of the Al distribution was calculated, and the results show a span of about 100 kJ/mol over the 64 different acid sites, which points to preferential Al location. The synthesis process needs to be taken into account in order to calculate Al distributions as the organic SDA, which fill the microporous channels, and the fluorine anions, which fill the D4R units interact with the Al atoms, making some sites more energetically favored. Both covalent and electrostatic factors take part in the total energy of the corresponding Al location. The overall Al populations show that 50% of the Al atoms are located in the D4R units. A model to calculate the hydroxyl populations is presented by first considering the Al incorporation (Si→Al substitution), taking into account the presence of the SDA, after which the protons are located in the four O of each AlO_4 tetrahedra with populations calculated from Boltzmann statistical factors. Relative peak areas are not well reproduced by our calculations, although this may be due to other factors. Preferential proton siting has also been studied in the H−ITQ-7 structure. Energy differences in each AlO_4 tetrahedra of about 30−40 kJ/mol are found, in qualitative agreement with ^1H NMR results, which indicate that large differences among populations of the four proton sites in an AlO_4 tetrahedra are expected.

Acknowledgment. We thank the Spanish CICYT (project MAT-2000-1392) for financial support; and C^4 (Centre de Computacio i Comunicacions de Catalunya) and Centro de Cálculo de la Universidad Politécnica de Valencia for the use of their computational facilities. We also thank Generalitat Valenciana for providing funds through the project GV01-492. The High Performance Computational Chemistry Group from Pacific Northwest National Laboratory (Richland, WA 993520999) is acknowledged for making available NWChem version 4.0, a computational chemistry package for parallel computers.

Supporting Information Available: Table I, calculated minimum energy conformation of ITQ-7 and four SDA molecules and Table II, calculated relative energy of Al in each T position of the ITQ-7 cell. This material is available free of charge via the Internet at http://pubs.acs.org.

References and Notes

(1) Rabo, J. A.; Kasai, P. H. *Prog. Solid State Chem.* **1975**, *9*, 1.
(2) Barthomeuf, D. *J. Phys. Chem.* **1979**, *83*, 249.
(3) Jacobs, P. A. *Catal. Rev. Sci. Eng.* **1982**, *24*, 415.
(4) Corma, A. *Chem. Rev.* **1995**, *95*, 559.
(5) Jentoft, F. C.; Gates, B. C. *Top. Catal.* **1997**, *4*, 1.
(6) Farneth, W. E.; Gorte, R. J. *Chem. Rev.* **1995**, *95*, 615.
(7) Sauer, J. *Chem. Rev.* **1989**, *89*, 199.
(8) Catlow, C. R. A.; Bell, R. G.; Gale, J. D. *J. Mater. Chem.* **1994**, *4*, 781.
(9) Senchenya, I. N.; Kazansky, V. B.; Beran, S. *J. Phys. Chem.* **1986**, *90*, 4857.
(10) Brand, H. V.; Curtiss, L. A.; Iton, L. E. *J. Phys. Chem.* **1992**, *96*, 7725.
(11) Zicovich-Wilson, C. M.; Dovesi, R. *Nuovo Cimento* **1997**, *19D*, 1785.
(12) van Santen, R. A.; Kramer, G. J. *Chem. Rev.* **1995**, *95*, 637.
(13) Jeanvoine, Y.; Angyan, J. G.; Kresse, G.; Hafner, J. *J. Phys. Chem. B* **1998**, *102*, 5573.
(14) Shah, R.; Gale, J. D.; Payne, M. C. *J. Chem. Soc., Chem. Commun.* **1997**, 131.
(15) Demuth, T.; Hafner, J.; Benco, L.; Toulhoat, H. *J. Phys. Chem. B* **2000**, *104*, 4593.
(16) Zicovich-Wilson, C. M.; Dovesi, R. *Chem. Phys. Lett.* **1997**, *277*, 227.
(17) *Modelling of Structure and Reactivity in Zeolites*; Catlow, C. R. A., Ed.; Academic Press: London, 1992.

(18) Sastre, G.; Fornes, V.; Corma, A. *J. Phys. Chem. B* **2000**, *104*, 4349.
(19) Shantz, D. F.; Fild, C.; Koller, H.; Lobo, R. F. *J. Phys. Chem. B* **1999**, *103*, 10858.
(20) Shantz, D. F.; Lobo, R. F.; Fild, C.; Koller, H. *Stud. Surf. Sci. Catal.* **2000**, *130*, 845.
(21) Shantz, D. F.; Schmedt auf der Günne, J.; Koller, H.; Lobo, R. F. *J. Am. Chem. Soc.* **2000**, *122*, 6659.
(22) Sabater, M. J.; Sastre, G. *Chem. Mater.* **2001**, *12*, 4520.
(23) Meier, W. M.; Olson, D. H.; Baerlocher, C.; *Atlas of Zeolite Structure Types*, 4th ed.; Elsevier: Amsterdam, 1996. Also in the URL http://www.iza-structure.org.
(24) Villaescusa, L. A.; Barrett, P. A.; Camblor, M. A. *Angew. Chem., Int. Ed. Engl.* **1999**, *38*, 1997.
(25) Corma, A.; Diaz-Cabañas, M. J.; Fornes, V. *Angew. Chem., Int. Ed. Engl.* **2000**, *39*, 2346.
(26) Corma, A.; Diaz, M. J.; Domine, M. E.; Rey, F. *Chem. Commun.* **2000**, 1725.
(27) Gale, J. D. *J. Chem. Soc., Faraday Trans.* **1997**, *93*, 629.
(28) Jackson, R. A.; Catlow, C. R. A. *Mol. Simul.* **1988**, *1*, 207. (b) Saul, P.; Catlow, C. R. A.; Kendrick, J. *Philos. Mag. B* **1985**, *51*, 107. (c) Schröder, K.-P.; Sauer, J.; Leslie, M.; Catlow, C. R. A.; Thomas, J. M. *Chem. Phys. Lett.* **1992**, *188*, 320. (d) Gale, J. D.; Henson, N. H. *J. Chem. Soc., Faraday Trans.* **1994**, *90*, 3175.
(29) Kiselev, A. V.; Lopatkin, A. A.; Shulga, A. A. *Zeolites* **1985**, *5*, 261.
(30) Oie, T.; Maggiora, T. M.; Christoffersen, R. E.; Duchamp, D. J. *Int. J. Quantum Chem., Quantum Biol. Symp.* **1981**, *8*, 1.
(31) Ditchfield, R.; Hehre, W. J.; Pople, J. A. *J. Chem. Phys.* **1971**, *54*, 724.
(32) Harrison, R.; Nichols, J.; Straatsma, T.; Dupuis, M.; Bylaska, E.; Fann, G.; Windus, T.; Apra, E.; Anchell, J.; Bernholdt, D.; Borowski, P.; Clark, T.; Clerc, D.; Dachsel, H.; de Jong, B.; Deegan, M.; Dyall, K.; Elwood, D.; Fruchtl, H.; Glendenning, E.; Gutowski, M.; Hess, A.; Jaffe, J.; Johnson, B.; Ju, J.; Kendall, R.; Kobayash, R.; Kutteh, R.; Lin, Z.; Littlefield, R.; Long, X.; Meng, B.; Nieplocha, J.; Niu, S.; Rosing, M.; Sandrone, G.; Stave, M.; Taylor, H.; Thomas, G.; van Lenthe, J.; Wolinski, K.; Wong, A.; Zhang, Z. "NWChem, A Computational Chemistry Package for Parallel Computers, Version 4.0" 2000, Pacific Northwest National Laboratory: Richland, WA 99352-0999.
(33) Henson, N. H.; Cheetham, A. K.; Gale, J. D. *Chem. Mater.* **1996**, *8*, 664.
(34) Sastre, G.; Lewis, D. W.; Catlow, C. R. A. *J. Phys. Chem.* **1996**, *100*, 6722. (b) Sastre, G.; Lewis, D. W.; Catlow, C. R. A. *J. Phys. Chem. B* **1997**, *101*, 4575.
(35) George, A. R.; Catlow, C. R. A. *Zeolites* **1997**, *18*, 67.
(36) Czjzek, M.; Jobic, H.; Fitch, A. N.; Vogt, T. *J. Phys. Chem.* **1992**, *96*, 1535.
(37) Sarv, P.; Tuherm, T.; Lippmaa, E.; Keskinen, K.; Root, A. *J. Phys. Chem.* **1995**, *99*, 13763.
(38) Fermann, J. T.; Blanco, C.; Auerbach, S. *J. Chem. Phys.* **2000**, *112*, 6779.